AFRL-RX-WP-TP-2010-4156

ATOMISTIC SIMULATIONS OF ATHERMAL CROSS-SLIP AT SCREW DISLOCATION INTERSECTIONS IN FACE-CENTERED CUBIC NICKEL (PREPRINT)

Satish I. Rao

UES, Inc.

Dennis M. Dimiduk, Michael D. Uchic, and Christopher Woodward

Metals Branch
Metals, Ceramics & NDE Division

Jaafar A. El-Awady

Universal Technology Corporation

JANUARY 2010

AIR FORCE RESEARCH LABORATORY
MATERIALS AND MANUFACTURING DIRECTORATE
WRIGHT-PATTERSON AIR FORCE BASE, OH 45433-7750
AIR FORCE MATERIEL COMMAND
UNITED STATES AIR FORCE

REPORT DOCUMENTATION PAGE

Form Approved
OMB No. 0704-0188

1. REPORT DATE *(DD-MM-YY)*	2. REPORT TYPE	3. DATES COVERED *(From - To)*
January 2010	Journal Article Preprint	01 January 2010 – 01 January 2010

4. TITLE AND SUBTITLE

ATOMISTIC SIMULATIONS OF ATHERMAL CROSS-SLIP AT SCREW DISLOCATION INTERSECTIONS IN FACE-CENTERED CUBIC NICKEL (PREPRINT)

5a. CONTRACT NUMBER
In-house

5b. GRANT NUMBER

5c. PROGRAM ELEMENT NUMBER
62102F

6. AUTHOR(S)

Satish I. Rao (UES, Inc.)
Dennis M. Dimiduk, Michael D. Uchic, and Christopher Woodward (AFRL/RXLM)
Jaafar A. El-Awady (Universal Technology Corporation)

5d. PROJECT NUMBER
4347

5e. TASK NUMBER
RG

5f. WORK UNIT NUMBER
M02R1000

7. PERFORMING ORGANIZATION NAME(S) AND ADDRESS(ES)

UES, Inc.
4401 Dayton-Xenia Road
Dayton, OH 45432-1894

Metals Branch (AFRL/RXLM)
Metals, Ceramics & NDE Division
Materials and Manufacturing Directorate
Wright-Patterson Air Force Base, OH 45433-7750
Air Force Materiel Command, United States Air Force

Universal Technology Corporation
1270 North Fairfield Road
Dayton, OH 45432-2600

8. PERFORMING ORGANIZATION REPORT NUMBER
AFRL-RX-WP-TP-2010-4156

9. SPONSORING/MONITORING AGENCY NAME(S) AND ADDRESS(ES)

Air Force Research Laboratory
Materials and Manufacturing Directorate
Wright-Patterson Air Force Base, OH 45433-7750
Air Force Materiel Command
United States Air Force

10. SPONSORING/MONITORING AGENCY ACRONYM(S)
AFRL/RXLMD

11. SPONSORING/MONITORING AGENCY REPORT NUMBER(S)
AFRL-RX-WP-TP-2010-4156

12. DISTRIBUTION/AVAILABILITY STATEMENT
Approved for public release; distribution unlimited.

13. SUPPLEMENTARY NOTES
Journal article submitted to *Philosophical Magazine*. PAO Case Number: 88ABW-2009-2917; Clearance Date: 29 Jun 2009. Paper contains color.

14. ABSTRACT

The Escaig model for thermally activated cross-slip in Face-Centered Cubic (FCC) materials assumes that cross-slip preferentially occurs at obstacles that produce large stress gradients on the Shockley partials of the screw dislocations. However, it is unclear as to the source, identity and concentration of such obstacles in single-phase FCC materials. In this manuscript, we describe embedded atom potential, molecular-statics simulations of screw character dislocation intersections with 120° forest dislocations in FCC Ni to illustrate a new mechanism for cross-slip nucleation. The simulations show how such intersections readily produce cross-slip nuclei and thus are preferential sites for spontaneous athermal cross-slip. The energies of the dislocation intersection cores are determined and it is shown that a partially cross-slipped configuration for the intersection is the most stable. In addition, simple 3-dimensional dislocation dynamics simulations accounting for Shockley partials are shown to qualitatively reproduce the atomistically-determined core structures for the same dislocation intersections.

15. SUBJECT TERMS

athermal cross-slip; dislocation intersections; atomistic simulations; embedded atom potentials; dislocation dynamics simulations

16. SECURITY CLASSIFICATION OF:			17. LIMITATION OF ABSTRACT:	18. NUMBER OF PAGES	19a. NAME OF RESPONSIBLE PERSON (Monitor)
a. REPORT	b. ABSTRACT	c. THIS PAGE			Christopher F. Woodward
Unclassified	Unclassified	Unclassified	SAR	42	19b. TELEPHONE NUMBER *(Include Area Code)* N/A

Standard Form 298 (Rev. 8-98)
Prescribed by ANSI Std. Z39-18

Atomistic Simulations of Athermal Cross-Slip at Screw Dislocation Intersections in Face-Centered Cubic Nickel

S.I. Rao*, D.M. Dimiduk, J.A. El-Awady#, T.A. Parthasarathy*, M.D. Uchic and C. Woodward

Air Force Research Laboratory, Materials and Manufacturing Directorate, AFRL/MLLM Wright-Patterson AFB, OH 45433-7817

*UES, Inc., 4401 Dayton-Xenia Rd, Dayton, OH 45432-1894

#UTC, Dayton, OH 45432

Abstract

The Escaig model for thermally activated cross-slip in Face-Centered Cubic (FCC) materials assumes that cross-slip preferentially occurs at obstacles that produce large stress gradients on the Shockley partials of the screw dislocations. However, it is unclear as to the source, identity and concentration of such obstacles in single-phase FCC materials. In this manuscript, we describe embedded atom potential, molecular-statics simulations of screw character dislocation intersections with 120^{o} forest dislocations in FCC Ni to illustrate a new mechanism for cross-slip nucleation. The simulations show how such intersections readily produce cross-slip nuclei and thus are preferential sites for spontaneous athermal cross-slip. The energies of the dislocation intersection cores are determined and it is shown that a partially cross-slipped configuration for the intersection is the most stable. In addition, simple 3-dimensional dislocation dynamics simulations accounting for Shockley partials are shown to qualitatively reproduce the atomistically-determined core structures for the same dislocation intersections.

Keywords: Athermal cross-slip; Dislocation intersections; Atomistic simulations; Embedded atom potentials; Dislocation dynamics simulations

1.0 Introduction

There is an increasing recognition and need to incorporate physics-based models of deformation in design of structural components. While models for predicting yield strength and creep behavior are beginning to incorporate significant physics, models for fatigue and ultimate strength remain mostly empirical. This is because strain-hardening and fatigue resistance are highly influenced by dislocation micromechanisms, especially cross slip and, including physics-based cross-slip processes in mesoscale simulations has been difficult. The early work of Escaig remains the most widely cited and used model for cross-slip (see figure 1); however, this model poses several difficulties with respect to quantitative simulations. The model is highly sensitive to choice of parameters that have thus far been difficult to obtain. For example, the constriction width required for cross-slip is unknown but significantly influences the energetics of the cross-slip process [1]. This difficulty has led to an ad-hoc postulate that obstacles always exist in materials and that they enable sufficient dislocation core constriction under normal stresses thereby ensuring cross-slip [2]. Aside from being unsatisfactory, this forces cross-slip models (particularly for single crystals) to make arbitrary assumptions about dislocation obstacle spacings. The advances in atomistic simulations have the possibility of helping to gain insights into the cross-slip process that may serve to inform mesoscale simulations to accurately capture the atomic-level physics of that dislocation process.

Atomistic simulation works to date have been limited to calculating constriction energies and energetics of cross-slip using a single dislocation in a periodic unit cell [3,4]. These simulations helped to unravel some interesting and useful aspects of cross-

slip thus far unanticipated. The most important finding was that there exist configurations where one of the pair of constrictions has a negative energy [3,4]. Thus spontaneous nucleation of cross-slip is possible so long as only one constriction is needed, as is the case for surface nucleation. However the total energy of a pair of constrictions, required for cross-slip within the bulk of a solid, is always positive. In particular, these simulations resulted in calculated energies for cross-slip (with two constrictions) that were so high (>1 eV) that thermal activation will be insufficient to activate them at temperatures where cross-slip is observed experimentally. This leaves the problem of having to assume ad-hoc obstacles in mesoscale simulations unchanged.

In this work, the possibility of cross-slip at dislocation-dislocation intersections was examined using large scale simulations that contain more than one dislocation. *A glide dislocation that intersects a pair of forest dislocations is modeled and it is shown that several conditions exist where cross-slip can nucleate spontaneously. This we believe has the potential of allowing simulations of cross-slip in larger scale discrete dislocation dynamics simulations to stand on a firm physical basis without ad-hoc assumptions and thus provides a realistic statistical representation of cross-slip during monotonic or cyclic deformation.*

We have performed molecular statics simulations of screw dislocation intersections with both the ½$[\bar{1}01]$ and the ½$[\bar{1}\,\bar{1}\,0]$ Burger's vectors on the $(1\,\bar{1}\,1)$ plane. We have considered several line orientations for the intersecting dislocation over a 180^o range (all orientations where the intersection is expected to be attractive). In this manuscript, for the sake of clarity, we restrict ourselves to results only for the screw dislocation intersection with the ½$[\bar{1}01]$ Burger's vector residing on the $(1\,\bar{1}\,1)$ plane with the

$120^o < 0\,\bar{1}\,\bar{1} >$ line orientation. Section 2 describes the simulation technique and the interatomic potential used for the simulations, Section 3 presents the core structures and the energies obtained from atomistic simulations and dislocation dynamics (DD) simulations for these specific intersections. Finally, Sections 4 and 5 give a discussion and summary of the results respectively.

2.0 Simulation technique

The atomistic simulations described here employed the 3-dimensional (3d) parallel molecular dynamics code, LAAMPS [5], developed at Sandia National Laboratory. A schematic of the simulation cell used in the atomistic simulations described in this manuscript is given in figure 2. The simulation cell is a rectangular parallelepiped cell, having the x-axis oriented along $[1\,\bar{1}\,0]$, y-axis along $[11\bar{2}]$ and the z-axis along [111]. The dimensions of the simulation cell were 62.0 nm along the x-axis and 31.5 nm along both the y- and z- axes corresponding to a simulation cell of 5,405,160 atoms. A $\frac{1}{2}[1\,\bar{1}\,0]$ screw dislocation is inserted in the middle of the simulation cell using its anisotropic elastic displacement field [6]. Two 120^o dislocations having a Burger's vector of $\frac{1}{2}[\bar{1}\,01]$ and line directions $< 0\,\bar{1}\,\bar{1} >$ spaced 30.0 nm apart (at x = -15.0 and 15.0 nm, with y, z ~0), were also introduced into the simulation cell using their anisotropic elastic displacement fields. The origin for the initial anisotropic displacement field of the screw and 120^o dislocations were varied (ten different origins were used) to obtain several different core structures for the screw dislocation intersection. For simplicity fixed boundary conditions were applied along all three directions and energy minimization was performed using the conjugate gradient technique. A couple of simulations were

performed using periodic boundary conditions along the screw or 'x' direction. In these cases, the two intersecting dislocations were opposite in character ($+120^o$ and -60^o), such that periodic boundary conditions could be applied.

2.1 Interatomic Potential

The embedded atom potential used in the simulations is the potential developed for FCC Ni by Angelo, Moody and Baskes [7] based on the Voter and Chen format. Table 1 gives the lattice parameter, cohesive energy, elastic constants and stacking fault energy given by the potential for FCC Ni. The stacking fault energy ~90 mJ/m^2, lies in between a value of 60 and 120 mJ/m^2, the values given by the two Ni potentials that Rao et. al., [3] used in previous atomistic simulations of bulk cross-slip.

2.2 Depiction of core structures

In order to illustrate the relaxed intersection geometries we take advantage of the increase in atomic energy produced by the strain field of the partial dislocations. By plotting the atoms with assigned energies within LAAMPs of greater than -4.42. eV (the energy of atoms in the stacking fault region) the partial dislocations can be imaged easily even in these large simulation cells. In order to illustrate the cross-slipped-segment products of the intersections the positions are shown in a $[11\bar{2}]$ projection (i.e. the x-z plane) as well as the [111] projection (i.e the x-y plane). In the $[11\bar{2}]$projection segments spread on the initial (111) plane appear as a single line and cross slipped segments (i.e. on a $(11\bar{1})$ plane) appear as a pair of partials separated by a stacking fault. The projection along the y axis provides a quick indicator of whether the screw dislocation is residing on the (111) glide plane or the $(11\bar{1})$ cross-slip plane or a combination of both.

2.2 Dislocation dynamics simulations

The core structures obtained for the intersection using atomistic simulations were reproduced using a simple Dislocation Dynamics (DD) method, DDLab, originally developed at Lawrence Livermore National Laboratory [8]. DDLab runs within MATLAB and is intended for simulations having a limited number of dislocation lines while taking into account the Shockley partials [9]. A ½$[1\bar{1}0]$ screw dislocation and a 120^o intersecting dislocation (Line direction $<0\bar{1}\bar{1}>$, Burger's vector ½$[\bar{1}01]$) split into their respective Shockley partials and fixed at both ends, were initially introduced into the simulation cell and allowed to relax under no applied stress. The screw character dislocation was initially taken to be either completely dissociated on the glide (111) plane, completely dissociated on the cross-slip $(11\bar{1})$ plane or, partly dissociated on the glide (111) plane and partly on the cross-slip $(11\bar{1})$ plane. The 120^o dislocation was initially taken to go through the origin of the simulation box whereas the screw dislocation was initially taken to be ± 0.8 nm away from the origin along the 'y' axis ($[11\bar{2}]$). The relaxed configurations were compared with results from atomistic simulations.

3.0 Core structures for the intersection

Figure 3 depicts [111] and $[11\bar{2}]$ projections (i.e. the 'x-y' and 'x-z' planes) of one of the core structures obtained for the screw dislocation–120^o dislocation intersection (Gl1). In this case, the screw dislocation was initially positioned a $[11\bar{2}]$ unit along the positive 'y' axis (+0.8nm), away from the origin. The original placement of the threading and

cutting dislocations allows the dislocation cores to interact and combine as dictated by the geometry and Peach Koehler forces as generated thorough the interatomic potentials. The screw dislocation fully resides on the glide (111) plane and is constricted at both the intersections (Stroh constrictions [10]) around one of the Shockley partials of the 120° ½[$\bar{1}$01] dislocation residing on the (1$\bar{1}\bar{1}$) plane. Due to the fixed boundary conditions along 'x' (which mimic a jog on the screw dislocation at the fixed boundaries), the screw dislocation is constricted in its glide plane at both ends near the boundary, which is equivalent to a full Stroh constriction [10]. Therefore, in order to obtain the true energy for the intersection core structure Gl1 without any jogs the energy of a 'Stroh' constriction needs to be subtracted from the energy of this core structure.

Figure 4 depicts two of the core structures obtained for the screw dislocation-120° dislocation intersection (LC1 and LC2). The [111] and [11$\bar{2}$] projections are shown for each case. In figure 3a, the screw dislocation was initially positioned a [11$\bar{2}$] unit along the positive 'y' axis (+0.8nm), away from the origin. In figure 3b, the screw dislocation was initially positioned a [11$\bar{2}$] unit along the negative 'y' axis (-0.8nm), away from the origin. After relaxation, figures 3a and 3b, the screw dislocation fully resides on the cross-slip (11$\bar{1}$) plane. In figure 3a, as in figure 1, the screw dislocation is constricted at both the intersections around one of the Shockley partials of the 120° ½[$\bar{1}$01] dislocation residing on the (1$\bar{1}$1) plane. In figure 3b, the a/6[$\bar{1}$12] Shockley partial of the screw dislocation combines with the a/6[1$\bar{2}\bar{1}$] Shockley partial of the 120° dislocation to form an extended node with a resulting short Burger's vector of the type 1/6[0$\bar{1}$1], Lomer Cottrell barrier. At the other end of the Lomer Cottrell barrier, the screw dislocation is constricted to form one half of a Stroh constriction. Since the interaction between the

1/6[$0\bar{1}1$] Burger's vector and the other Shockley partial of the 120° dislocation (a/6[$2\bar{1}1$]) is weak, the 120° dislocation needs to constrict significantly to attain a lower separation distance at the extended node reaction region. Also, as in figure 3, due to the fixed boundary conditions along 'x', the screw dislocation forms an equivalent of a 'Stroh' constriction at its ends and this energy has to be subtracted to obtain the true energy of intersection core structures LC1 and LC2 without any jogs.

Figure 5 depicts two of the core structures obtained for the screw dislocation-120° dislocation intersection (PCS1 and PCS2). The [111] and [$11\bar{2}$]' projections are shown for each case. In figure 5a, the screw dislocation was initially positioned a [$11\bar{2}$] unit along the positive 'y' axis (+0.8nm), away from the origin. In figure 5b, the screw dislocation was initially positioned a [$11\bar{2}$] unit along the negative 'y' axis (-0.8nm), away from the origin. In both cases, the screw dislocation is partially on the glide (111) plane and partially on the cross-slip ($11\bar{1}$) plane. This is in essence the athermal presence of cross-slip nucleii at these intersections. These results are similar to previous observations of athermal cross-slip at screw dislocation interactions with Frank interstitial loops in FCC Ni [11]. In figure 4a, as in figure 1, the screw dislocation is constricted at both the intersections (negative constrictions [3,4]) around one of the Shockley partials of the 120° ½[$\bar{1}01$] dislocation residing on the ($1\bar{1}1$) plane. Since the core is in the partially cross-slipped state, a companion positive constriction [3, 4] forms between the intersections. In figure 5b, as in figure 4b, a/6[$\bar{1}12$] Shockley partial of the screw dislocation combines with the a/6[$1\bar{2}\bar{1}$] Shockley partial of the 120° dislocation to form an extended node with a resulting short Burger's vector of the type 1/6[$0\bar{1}1$], Lomer

Cottrell barrier. At the other end of the Lomer Cottrell barrier, the screw dislocation is constricted to form one half of a negative constriction and is cross-slipped onto the glide (111) plane. Since the core is in the partially cross-slipped state, a companion full positive constriction [3, 4] forms between the intersections. As in figure 4b, since the interaction between the $1/6[0\bar{1}1]$ Burger's vector and the other Shockley partial of the 120^o dislocation is weak, the 120^o dislocation needs to constrict significantly to attain a lower separation distance at the extended node reaction region. Due to the fixed boundary conditions along 'x', the screw dislocation is constricted at both ends near the boundary in both figures. 5a and 5b, forming what is equivalent to a full positive constriction [3, 4]. In this case, this behavior can be interpreted as the natural formation of a positive constriction in between intersections and no energy correction is required to obtain the energy of core structures PCS1 and PCS2.

3.1 Energetics of the intersection core structures

Since the core of the intersecting dislocations pass through the fixed boundary along 'y' and 'z', the energy differences of corresponding atoms between different core structures is subject to large errors, especially near the boundary. Therefore, the energy difference evaluations were truncated at different distances along 'y' and 'z' starting from the center. Figure 6 is a plot of the relative energy of three different core structures obtained for the screw–120^o intersection as a function of the distance along 'y' and 'z' taken into consideration in the evaluation. The whole length of relaxed region along 'x' is taken into account in evaluating the energy differences. Along 'y' and 'z', the energy evaluation is truncated at 5.0, 7.5, 10.0 and 12.5 nm, and the energy difference obtained

between the different core structures is plotted as a function of this truncated distance. Curve (a) in figure 6 is a plot of the energy differences between two identical core structures obtained for the intersection (Figure 3, fully residing on the glide (111) plane) with two different initial elastic centers and shows that the measurement of relative energy has an error of the order of 0.2 eV using this technique. The partially cross-slipped configuration (PCS1) is stable relative to the cores Gl1 (fully residing on the glide plane) and LC2 (fully residing on the cross-slip plane) by 4 - 4.6 eV and the energy difference values are fairly converged at a distance of 125 A along 'y' and 'z'. If one subtracts the bulk Stroh constriction energy from the energy of the core structures Gl1 and LC2, for reasons stated in Section 3.0, (~1.9 eV, estimated from [3] as a mean of the negative and positive constriction energies at a stacking fault energy of 90 mJ/m^2), one obtains that the partially cross-slipped configuration is stable relative to Gl1 and LC2 by 2.1 - 2.7 eV, giving a value of 1 - 1.3 eV stability per intersection. These results suggest that the energy of a negative constriction is significantly depressed at the intersections, relative to the bulk, due to the stress field of the intersecting dislocations. Table 2 gives the relative energy values for the five different core structures shown in figures 3 - 5 obtained using the technique described above with a truncation distance along 'y' and 'z' of 12.5 nm, without the Stroh constriction correction. These results suggest that cross-slip nuclei are readily available at these intersections and that cross-slip at these intersections is athermal and spontaneous in FCC Ni. Also, the energy of core structures with extended nodes (obtained when the screw dislocation was initially placed a [112] unit along the negative 'y' axis, LC1 and PCS2) is significantly larger than the core structures which have no extended nodes (obtained when the screw dislocation was

initially placed a [112] unit along the positive 'y' axis, Gl1, LC2 and PCS1). This may be related to the constriction of the 120^o dislocations that is required to form the extended node.

3.2 Periodic boundary condition simulations

A couple of simulations were performed imposing periodic boundary conditions along the screw (x or $1\bar{1}0$) direction. Such boundary conditions could be imposed only by making the two intersecting dislocations opposite or dipole in character (+120^o and -60^o). Fixed boundary conditions were still imposed along the 'y' and 'z' directions. Figure 7 is a plot of two different core structures obtained for the intersection using four different elastic centers for the initial anisotropic displacement field, with periodic boundary conditions imposed along the 'x' direction. In both cases, the screw dislocation is partially cross-slipped onto the cross-slip $(11\bar{1})$ plane. In figure 7a, the screw dislocation is partially cross-slipped at the +120^o intersection whereas in figure 7b, it is partially cross-slipped at both the +120^o and -60^o intersections. These results suggest that the partially cross-slipped configuration forms even at the repulsive -60^o intersection.

3.3 Dislocation dynamics simulations

Figure 8 gives a plot of the structure of a 120^o intersection core obtained using 3d dislocation dynamics simulations. The dislocation dynamics simulation results are compared with the corresponding core structure obtained for the 120^o intersection with

atomistic simulations. In figure 8, the screw dislocation was initially placed in the 3d dislocation dynamics simulation cell as partially cross-slipped onto the cross-slip $(11\bar{1})$ plane. The node transitioning the screw dislocation from the (111) glide plane to the cross-slip $(11\bar{1})$ plane was free to move along the screw $[1\bar{1}0]$ direction. Figure 8 shows that the partially cross-slipped configuration for the 120^o intersection core is stable and good correspondence is found between the dislocation dynamics and atomistic simulation results. We conclude that the elastic interactions of the partial dislocations and the ensuing recombination of the partials at the junctions captures the essential details of the dislocation evolution within the atomistic simulations. This reaction pathway is controlled by the partial dislocations, and not some nuance of the local atomic structure. Similar dislocation dynamics simulations were found to reproduce all the five core structures (figures 3 - 5) obtained for the 120^o intersection atomistically.

4.0 Discussion

The results of this work clearly show that several dislocation configurations exist within FCC crystals containing forest dislocations, where a glide dislocation can spontaneously nucleate a cross-slip event. This is an important result since it qualitatively justifies the profuse nature of cross slip in FCC crystals, unlike the current models for thermally-activated cross slip that so far require too high of energy to provide a self-consistent explanation. This finding should allow higher-level mesoscale models of dislocation behavior to better represent the cross-slip process without resort to ad hoc assumptions about obstacles. The results and their importance are discussed further in the following, starting with the state-of-the-art in cross-slip models.

Most mesoscale models to date that include cross-slip employ the Escaig model. The thermally activated continuum Escaig model for cross-slip in FCC materials [2,12-14] assumes that cross-slip preferentially occurs at obstacles yielding a very large stress gradient at the Shockley partials of the screw dislocations. The activation energy for cross-slip at a pre-existing constriction (Stroh constriction) is determined to be

$$W = \frac{A\mu b^2}{8\pi} d_0[(1-\frac{b_0}{d_0})^2 - \alpha_1 \frac{\tau b}{\gamma}]$$
$$\alpha_1 = 1.6\alpha^{'} + [1.6 - \frac{1}{2\sqrt{3}}(1-\frac{b_0}{d_0})^2]\alpha^{''} + 2.77 \qquad (1)$$

where τ is the resolved shear stress acting on the screw dislocation on the glide plane, $\alpha'\tau$ is the widening shear stress (Escaig stress) on the glide plane, $\alpha^{''}\tau$ is the widening shear stress on the cross-slip plane, $d_0 = \mu b^2/16\pi\gamma$, μ is the shear modulus, γ is the stacking fault energy, b_0 is the conventional width attributed to the recombined perfect screw dislocation, and A ~$0.92[\ln(\mu b/15\gamma)]^{1/2} - 0.60$. At zero stress, the activation energy is the energy required to separate a pre-existing constriction (Stroh constriction) into two fully formed constrictions, a) a negative constriction that takes the dislocation from the glide plane to the cross-slip plane [3, 4] and b) a positive constriction that takes the dislocation from the cross-slip plane to the glide plane as shown in figure 1 [3, 4]. Most continuum analyses makes two assumptions: 1) that all three constrictions, Stroh, negative and positive are identical to each other and 2) since the leading Shockley of the screw dislocation is assumed to be blocked at an obstacle, the resolved shear stress on the glide plane constricts the core of the screw dislocation significantly thereby making cross-slip feasible at a fairly low applied stress (of the order of τ_{III} [2]).

Previous atomistic simulations of constrictions in bulk Cu and Ni [3, 4] have shown that the energies of the negative and positive constrictions are completely different from each other. From these simulations it was shown that the negative constriction has a negative energy (with respect to a fully spread out Shockley partial configuration) while the positive constriction has a large positive energy. However, the sum of the negative and positive constriction energies is positive, finite, and depends on the initial Shockley partial spacing of the screw dislocation or the stacking fault energy. The energy of the Stroh constriction can be shown to be a mean of the energies of the negative and positive constrictions [15]. Therefore, since both the negative and positive constrictions have to form from a pre-existing Stroh constriction for cross-slip to occur in the bulk, the cross-slip energy is positive and finite and thermally activated, in agreement with Escaig's model. However, for example, since only a single constriction has to form for cross-slip to occur at a surface, cross-slip can be spontaneous at a free surface. This conjecture is in agreement with atomistic simulation results for surface cross-slip, to be published in a forthcoming manuscript [16]. Also, the energies of the constrictions that form at screw dislocation intersections with other forest dislocations is not known and could be completely different from those in bulk. Thus, in Escaig's model the identity and concentration of the obstacles needs to be identified for otherwise pure single-phase FCC materials containing only dislocation debris. The definition of such obstacles is uncertain making the continuum determination of the stress-dependence of the cross-slip activation energy problematic [17].

In the early 1960's, Washburn [18] suggested that cross-slip in FCC materials preferentially occurs at dislocation intersections with other forest dislocations residing on

the cross-slip plane that form collinear locks and glide locks [18, 19]. For these configurations the dislocation has to pass through the screw orientation for the intersection product to form and the dislocation has to essentially form one single new constriction for this mechanism to operate. However, in Escaig's bulk cross-slip model as well, on an average, a single new constriction has to form for cross-slip to occur. Also, the length of dislocation that passes through the screw orientation when the intersection product is formed is minimal and is not readily amenable for cross-slip. Therefore, if one only considers screw dislocation intersections with forest dislocations on the cross-slip plane, it is possible that the intersection energies are such that cross-slip can be easily initiated at these intersections. However, for the case of forest dislocations on the cross-slip plane, if cross-slip occurs at the intersections taking the screw dislocation from the glide to the cross-slip plane locally, the cross-slipped product will not be stable since it can react with the forest dislocation on the cross-slip plane to form a new reaction product with a different Burger's vector.

In this work, we expanded on the idea of Washburn. We considered screw dislocation intersections with forest dislocations residing on the two other {111} type planes, other than forest dislocations residing on the cross-slip {111} type plane. If we take the screw dislocation as having a $\frac{1}{2}[1\bar{1}0]$ Burger's vector residing on the (111) plane with the $(11\bar{1})$ plane being the cross-slip plane, then for reasons stated above, the intersections that are of importance for cross-slip are intersections with the $(1\bar{1}1)$ and $(1\bar{1}\bar{1})$ planes. Table 3 gives the locks that are formed as well as the reaction product, for intersections with different Burger's vectors on these two planes as well as the cross-slip plane. In Table 3, the locks that are formed are written down for two cases: 1) the screw

dislocation is completely residing on the glide (111) plane and 2) the screw dislocation is completely residing on the cross-slip $(11\bar{1})$ plane. From Table 3, it is clear, that by symmetry, the intersections with the $(1\bar{1}1)$ plane are identical to the intersections with the $(1\bar{1}\bar{1})$ plane, and therefore, one needs to consider only the screw dislocation intersections with the $(1\bar{1}1)$ plane. Also, considering that the screw dislocation can completely reside on the glide (111) or the cross-slip $(11\bar{1})$ plane, the intersection with the ½$[\bar{1}01]$ Burger's vector on the $(1\bar{1}1)$ plane can be shown by symmetry to be equivalent to the intersection with the ½[011] Burger's vector on the $(1\bar{1}1)$ plane. As a result, one needs to consider only the intersections with the ½$[\bar{1}01]$ and the ½$[\bar{1}\bar{1}0]$ Burger's vectors on the $(1\bar{1}1)$ plane. For the ½$[\bar{1}01]$ Burger's vector, the intersection results in a Lomer-Cottrell barrier if the screw dislocation is on the cross-slip $(11\bar{1})$ plane or, a glide barrier if the screw dislocation is residing on the glide (111) plane. For the ½$[\bar{1}\bar{1}0]$ Burgers vector, the intersection results in a Hirth lock irrespective of whether the screw dislocation resides on the glide plane or the cross-slip plane. The common direction (junction direction) between the screw direction glide plane, (111) and the intersecting $(1\bar{1}1)$ plane is $[\bar{1}01]$ and the common direction between the screw direction cross-slip plane, $(11\bar{1})$ and the $(1\bar{1}1)$ plane is [011]. Due to the fact that the junction direction as well as the type of lock that is formed is dependent on whether the screw dislocation resides on the glide plane or the cross-slip plane, the energetics of these intersections may be expected to depend strongly on the plane in which the screw dislocation resides. This may enhance the possibility of local cross-slip at the intersection region.

These atomistic simulation results suggest that cross-slip nuclei are readily available at screw dislocation intersections with forest dislocations residing on the two {111} planes other than the cross-slip plane forming either Lomer-Cottrell, Glide or Hirth locks. Cross-slip at these intersections is athermal and spontaneous and should be feasible even at no or very low applied stress. This is unlike Escaig's model where cross-slip is thermally activated and strongly applied stress dependent. Within this mechanism, the frequency of cross-slip in FCC materials should scale with the forest dislocation density. The relative magnitude of local stresses on the glide plane and the cross-slip plane at the partially cross-slipped screw dislocation intersection region should make the core move toward being completely on the glide plane or cross-slip plane. Such behavior of the partially cross-slipped core under different modes of applied stress must be studied using atomistic simulations. Since cross-slip is athermal within this mechanism, the magnitude of stacking fault energy should have a minimal effect on the cross-slip frequency. This is because the negative value of the energy of the negative constriction is mainly due to line energy anisotropy in FCC materials with Poisson's ratio of the order of 0.3 - 0.4 [3,4]. Nevertheless, atomistic simulations of these screw dislocation intersection core structures in other FCC materials with different stacking fault energies like Al, Cu must be performed to verify the results in Ni as well as determine the energy well for the partially cross-slipped intersection core configuration as a function of stacking fault energy. This intersection mechanism of cross-slip must be implemented in 3d dislocation dynamics simulations as an alternative to Escaig's model to study dislocation structure evolution with strain in FCC materials since it overcomes the difficulties of the Escaig model; namely, the obstacle hypothesis [17]. Finally, the Bonneville and Escaig

experimental results on cross-slip in FCC Cu should be reinterpreted taking into account of this intersection mechanism for cross-slip [2, 20].

Within this mechanism of intersection cross-slip, according to Washburn [18], double intersection cross-slip, where the segment that has been pulled into the cross-slip plane soon encounters another attractive intersection that pulls it back into a new layer of the primary glide plane, provides a reasonable mechanism for dislocation multiplication and the growth of slip bands at low temperatures. Also, classical theories of work-hardening assume that dislocation storage in Stage II of single-crystal fcc materials is a result of junction formation [21] or 2-dimensional concave loop formation [22] as the gliding dislocation traverses through an array of forest dislocation obstacles on its glide plane. However, one of the major problems in classical strain-hardening models is how to explain the generation of a three-dimensional network of stored dislocations as a consequence of two-dimensional glide [22]. We note that the athermal intersection cross-slip mechanism for dislocation storage provides a convenient mechanism of generating a three-dimensional network of stored dislocations from two-dimensional glide.

5.0 Summary

The simulations in this work show that the nucleation of cross-slip can be spontaneous during dislocation-dislocation interactions and that atomistic simulations can be used to identify types of interactions that result in cross-slip and use in higher level mesoscale simulations. Summarizing the results, for a 120^{o} $\frac{1}{2}[\bar{1}01]$ Burgers vector, $<0\bar{1}\bar{1}>$ line direction dislocation residing on the $(1\bar{1}1)$ plane intersecting a $\frac{1}{2}[1\bar{1}0]$

screw dislocation, the following observations were made using atomistic simulations of the intersection core structure using embedded atom potentials:

1) Five different core structures were obtained for the intersection with the screw dislocation fully residing on the glide (111) plane in one core structure, fully residing on the $(11\bar{1})$ cross-slip plane in two other core structures and partially residing on both the glide (111) and cross-slip $(11\bar{1})$ in the final two core structures.

2) One of the partially cross-slipped configuration for the core structure of the intersection is stable relative to the other two core structures (residing either fully on glide (111) or fully on cross-slip $(11\bar{1})$ plane) by 1.1 - 1.3 eV per intersection.

3) The extended node structure for the intersections is relatively unstable with respect to the constricted structure, presumably due to the formation of significant constriction on the 120^o intersecting dislocation.

4) Dislocation dynamics simulations accounting for Shockley partials are shown to reproduce the products of dislocation intersections interacting at the atomistic level. The reaction pathway for the cross slipped nuclei are controlled by elastic interactions and recombination of the partial dislocations.

ACKNOWLEDGEMENT

The authors acknowledge use of the 3d molecular dynamics code, LAAMPS, which was developed at Sandia National Laboratory by Dr. Steve Plimpton and co-workers. The authors also acknowledge use of the 'Matlab' version of 3d dislocation dynamics code, ParaDiS, which was developed at Lawrence Livermore National Laboratory by the ParaDiS team. This work was supported by the AFOSR, and by a grant of computer time

from the DOD High Performance Computing Modernization Program, at the Aeronautical Systems Center/Major Shared Resource Center. The work was performed at the U.S. Air Force Research Laboratory, Materials and Manufacturing Directorate, Wright-Patterson AFB.

REFERENCES

1. G. Saada, Mater.Sci. and Engr., **A137**, 177 (1991).
2. J. Bonneville and B. Escaig, Acta Metallurgica, **27**, 1477 (1979).
3. S. Rao, T.A. Parthasarathy and C. Woodward, Phil.Mag.A, **79**, 1167 (1999).
4. T. Rasmussen, K.W. Jacobsen, T. Leffers and D.B. Pedersen, Phys.Rev.B, **56**, 2977 (1997).
5. S.J. Plimpton, J.Comp.Phys., **117**, 1 (1995).
6. A.N. Stroh, Phil. Mag., **3**, 625 (1959).
7. J.E. Angelo, N. R. Moody and M.I. Baskes, Modell. Simul. Mater. Sci. Eng., **3**, 289 (1995).
8. V. Bulatov and W. Cai, Computer Simulations of Dislocations, v**3**, Oxford University Press, Oxford (2006).
9. E. Martinez, J. Marian. A. Arsenlis, M. Victoria and J.M. Perlado, Jour. of the Mechanics and Physics of Solids, **56**, 869 (2008).
10. A. N. Stroh, Proc. Phys. Soc. B, **67**, 427 (1954).
11. D. Rodney, Acta Materialia, **52,** 607 (2004).
12. B. Escaig, Proceedings of the Battelle Colloquium on Dislocation Dynamics, edited by A.R. Rosenfield, G.T. Hahn, A.L. Bement Jr., and R.I. Jaffee (New York : McGraw-Hill), 655 (1968).
13. W. Puschl, Prog. Mater. Sci., **47**, 415 (2002).

14. D. Caillard and J.L. Martin, 'Thermally activated mechanisms in Crystal Plasticity', Pergamon-Elsevier, Amsterdam (2003).

15. S. Rao, unpublished calculations (2009).

16. S. Rao, D.M. Dimiduk, El-Awady Jaafar, T.A. Parthasarathy, M.D. Uchic and C. Woodward, to be published (2009).

17. L. Kubin, T.Hoc and B. DeVincre, Acta Materialia, (2009), available online at www.sciencedirect.com.

18. J. Washburn, Appl. Phys. Letters, **7**, 183 (1965).

19. B. Madec, B. DeVincre and L. P. Kubin, Phys. Rev. Letters, **89**, 255508 (2002).

20. J. Bonneville, B. Escaig and J.L. Martin, Acta Metallurgica, **36,** 1989 (1988).

21. B. DeVincre, T. Hoc and L. Kubin, Science, **320**, 1745 (2008).

22. U.F. Kocks and H. Mecking, Progress in Materials Science, **48**(3), 102 (2003).

Figure captions

Figure 1: Illustration of the activation energy for cross-slip in Escaig's model: separation of a Stroh constriction into a negative and a positive constriction.

Figure 2: A schematic of the simulation cell used in the atomistic simulations described in this manuscript.

Figure 3: [111] (X-Y plane) and $[11\bar{2}]$ (X-Z plane) projections of the core structure (Gl1) for a screw-120^0 intersection in FCC Ni from atomistic simulations. Atoms with an energy greater than their energy at a stacking fault are plotted.

Figure 4: [111] (X-Y plane) and $[11\bar{2}]$ (X-Z plane) projections of the core structures (LC1 and LC2) for a screw-120^0 intersection in FCC Ni from atomistic simulations. Atoms with an energy greater than their energy at a stacking fault are plotted.

Figure 5: [111] (X-Y plane) and $[11\bar{2}]$ (X-Z plane) projections of the core structures (PCS1 and PCS2) for a screw-120^0 intersection in FCC Ni from atomistic simulations. Atoms with an energy greater than their energy at a stacking fault are plotted.

Figure 6: Relative energies of the core structures, Gl1, LC2 and PCS1, plotted as a function of the truncation distance along 'y' and 'z'. Two instantiations of the core

structure Gl1 are also compared with each other to determine the accuracy in the relative energy measurement.

Figure 7: [111] (X-Y plane) and $[11\bar{2}]$ (X-Z plane) projections of two different core structures obtained for a screw-120^0 - -60^o intersection in FCC Ni from atomistic simulations with periodic boundary conditions along the screw or 'x' direction. Atoms with an energy greater than their energy at a stacking fault are plotted.

Figure 8: A comparison of the dislocation dynamics results for the partially cross-slipped core structure of a screw-120^0 intersection, with atomistic simulation results. [111] (X-Y plane) and $[11\bar{2}]$ (X-Z plane) projections are shown for each case.

Property	**Value**
a_0	3.52 A
C_{11}	2.464 x 10^{12} dynes/cm^2
C_{12}	1.473 x 10^{12} dynes/cm^2
C_{44}	1.248 x 10^{12} dynes/cm^2
E_c	-4.45 eV
γ	89 mJ/m^2

Table 1: Lattice parameter, a_0; Cohesive energy, E_c; Elastic constants C_{11}, C_{12} and C_{44}; and stacking fault energy, γ, given by the Ni Angelo, Moody and Baskes EAM potential.

Core	**Relative energy (eV)**
GL1	0
LC1	5.3
LC2	-0.8
PCS1	-4.6
PCS2	5.8

Table 2: Relative energies of various core structures obtained atomistically for the screw dislocation – 120^{o} dislocation intersection.

Plane	Burgers Vector	Reaction	Lock Glide Cross-slip
$11\bar{1}$	$-\frac{1}{2}[1\bar{1}0]$	$\frac{1}{2}[1\bar{1}0]-\frac{1}{2}[1\bar{1}0]=0$	Collinear Annihilation
$11\bar{1}$	$-\frac{1}{2}[101]$	$\frac{1}{2}[1\bar{1}0]-\frac{1}{2}[101]=\frac{1}{2}[0\bar{1}\bar{1}]$	Glide Reaction
$11\bar{1}$	$\frac{1}{2}[011]$	$\frac{1}{2}[1\bar{1}0]+\frac{1}{2}[011]=\frac{1}{2}[101]$	Glide Reaction
$1\bar{1}1$	$-\frac{1}{2}[110]$	$\frac{1}{2}[1\bar{1}0]-\frac{1}{2}[110]=[0\bar{1}0]$	Hirth Hirth
$1\bar{1}1$	$-\frac{1}{2}[10\bar{1}]$	$\frac{1}{2}[1\bar{1}0]-\frac{1}{2}[10\bar{1}]=\frac{1}{2}[0\bar{1}1]$	Glide Lomer Cottrell
$1\bar{1}1$	$\frac{1}{2}[011]$	$\frac{1}{2}[1\bar{1}0]+\frac{1}{2}[011]=\frac{1}{2}[101]$	Lomer Cottrell Glide
$1\bar{1}\bar{1}$	$-\frac{1}{2}[110]$	$\frac{1}{2}[1\bar{1}0]-\frac{1}{2}[110]=[0\bar{1}0]$	Hirth Hirth
$1\bar{1}\bar{1}$	$-\frac{1}{2}[101]$	$\frac{1}{2}[1\bar{1}0]-\frac{1}{2}[101]=\frac{1}{2}[0\bar{1}\bar{1}]$	Lomer Cottrell Glide
$1\bar{1}\bar{1}$	$\frac{1}{2}[01\bar{1}]$	$\frac{1}{2}[1\bar{1}0]+\frac{1}{2}[01\bar{1}]=\frac{1}{2}[10\bar{1}]$	Glide Lomer Cottrell

Table 3: Reactions and locks that occur between a $\frac{1}{2}[1\bar{1}0]$ screw dislocation and forest dislocations on the $(11\bar{1})$, $(1\bar{1}1)$ and $(1\bar{1}\bar{1})$ planes. The screw dislocation is considered to reside completely, either on the glide (111) or the cross-slip $(11\bar{1})$ plane.

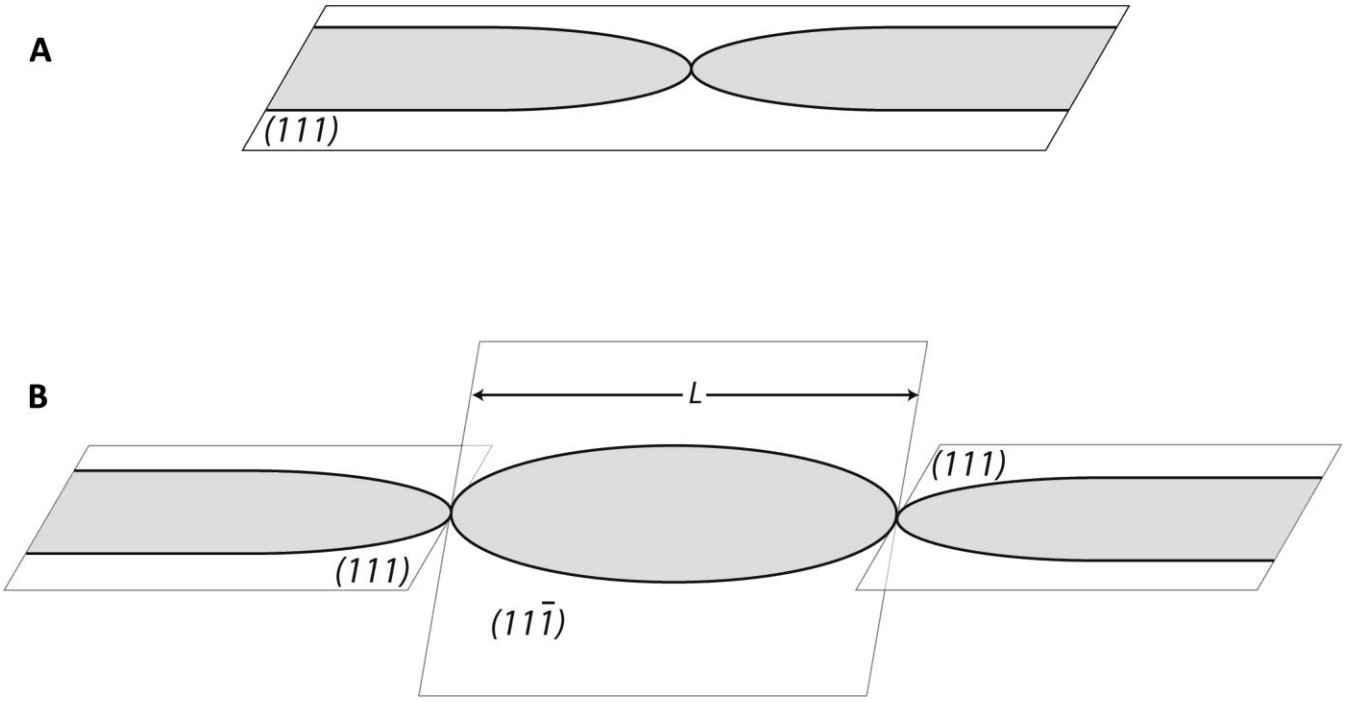

Fig.1:

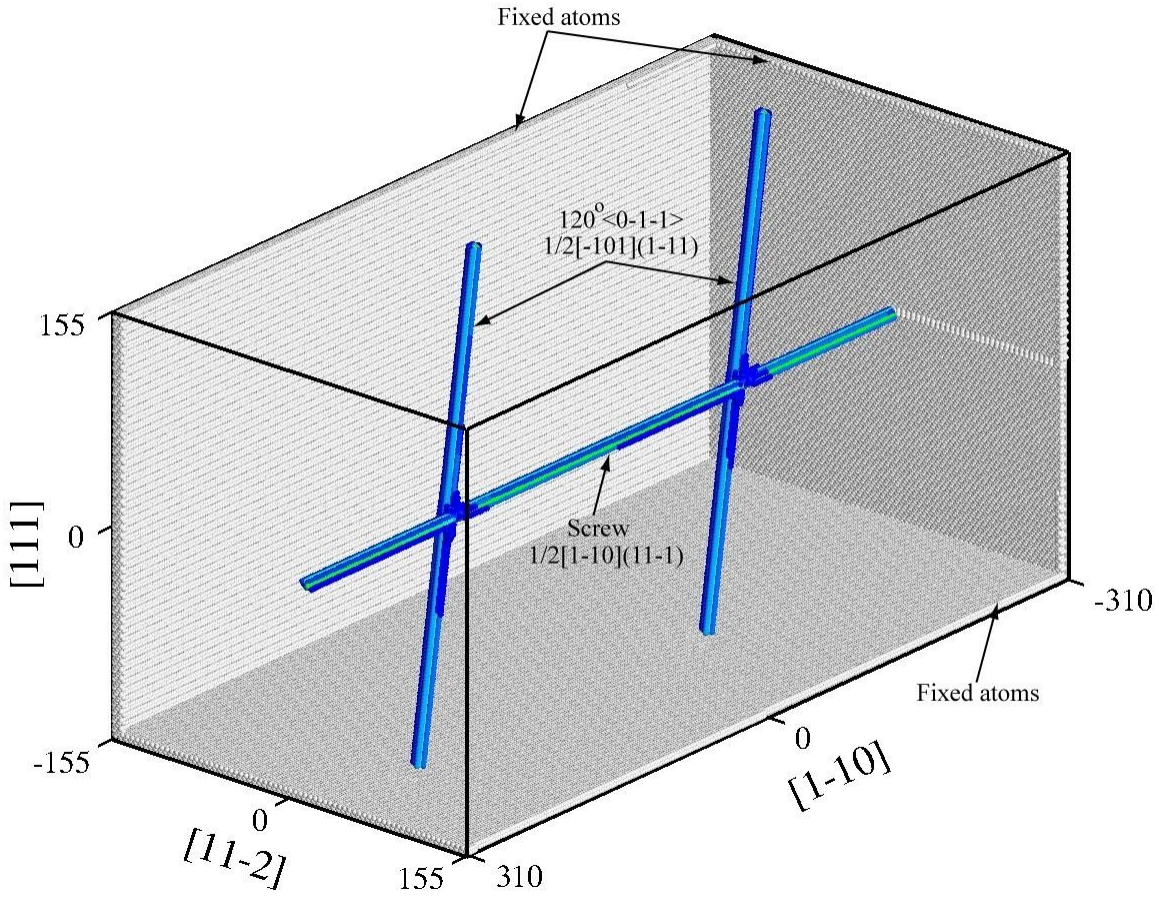
Fixed atoms
120°<0-1-1>
1/2[-101](1-11)
155
0
[111]
-155
Screw
1/2[1-10](11-1)
-310
Fixed atoms
0
[1-10]
0
[11-2]
155
310

Fig.2:

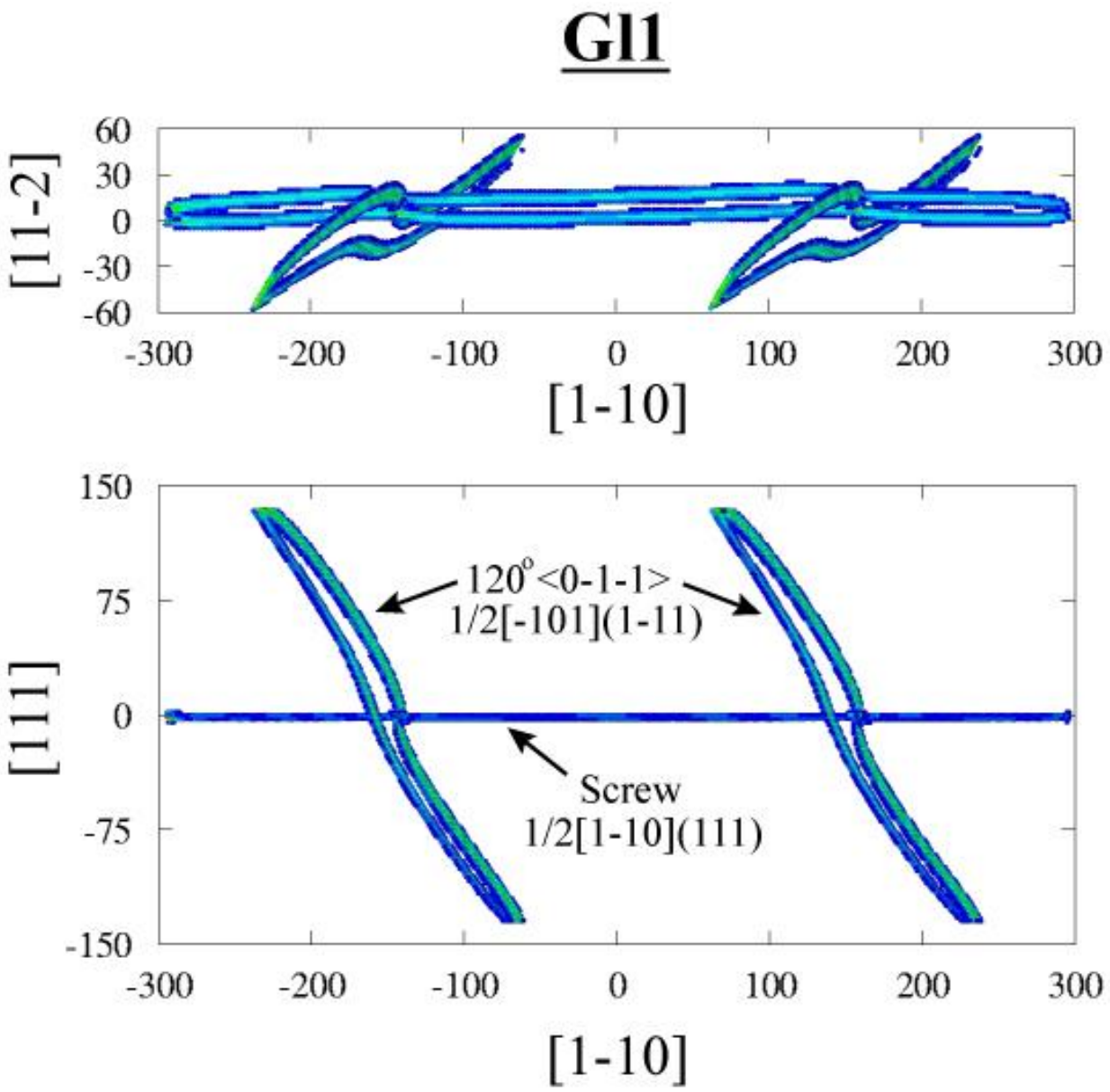
Gl1
[11-2]
60
30
0
-30
-60
-300
-200
-100
0
100
200
300
[1-10]
[111]
150
75
0
-75
-150
120°<0-1-1>
1/2[-101](1-11)
Screw
1/2[1-10](111)
-300
-200
-100
0
100
200
300
[1-10]

Fig.3:

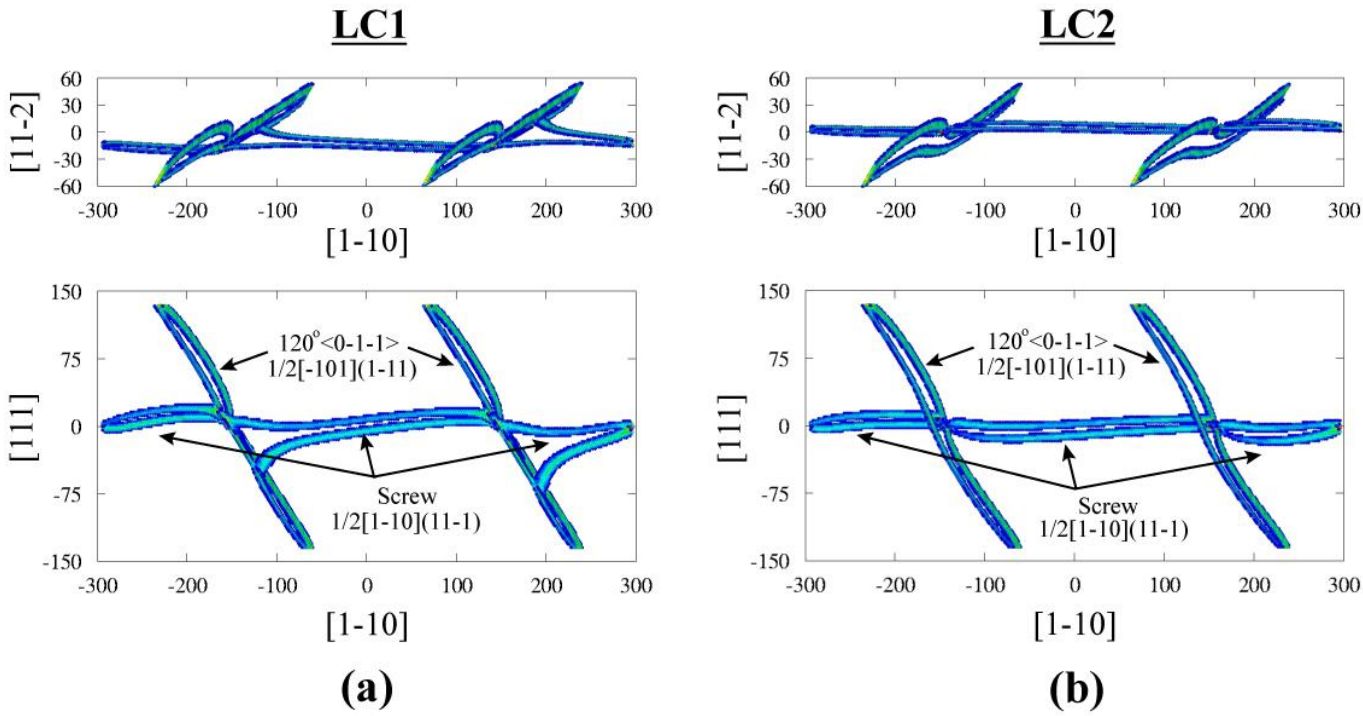

Fig.4:

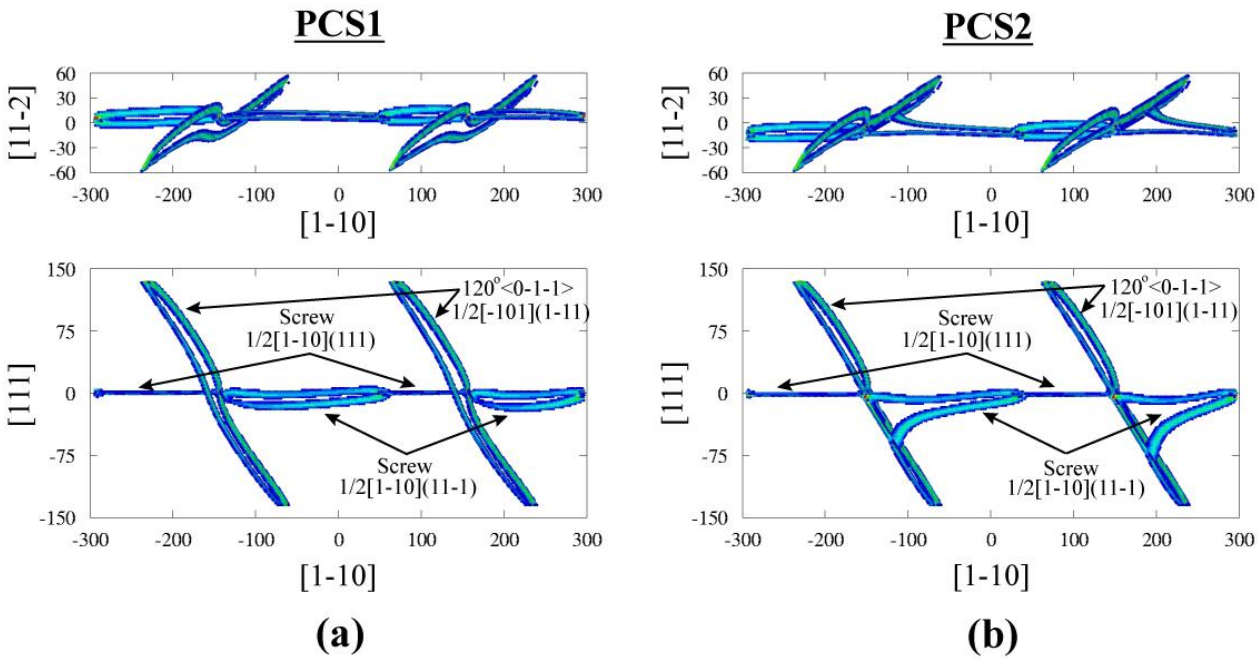
PCS1
PCS2
[11-2]
[1-10]
[111]
120°<0-1-1>
1/2[-101](1-11)
Screw
1/2[1-10](111)
Screw
1/2[1-10](11-1)
(a)
(b)

Fig. 5:

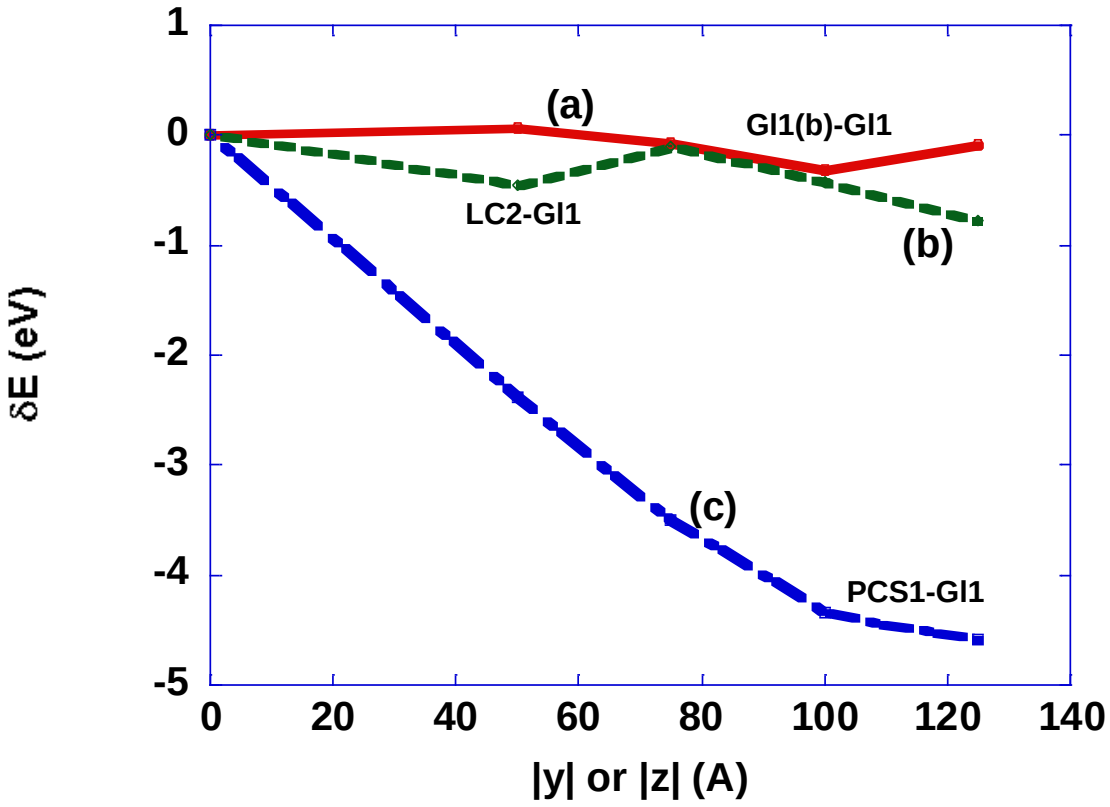
1
0
-1
-2
-3
-4
-5
0
20
40
60
80
100
120
140
δE (eV)
|y| or |z| (A)
(a)
Gl1(b)-Gl1
LC2-Gl1
(b)
(c)
PCS1-Gl1

Fig.6:

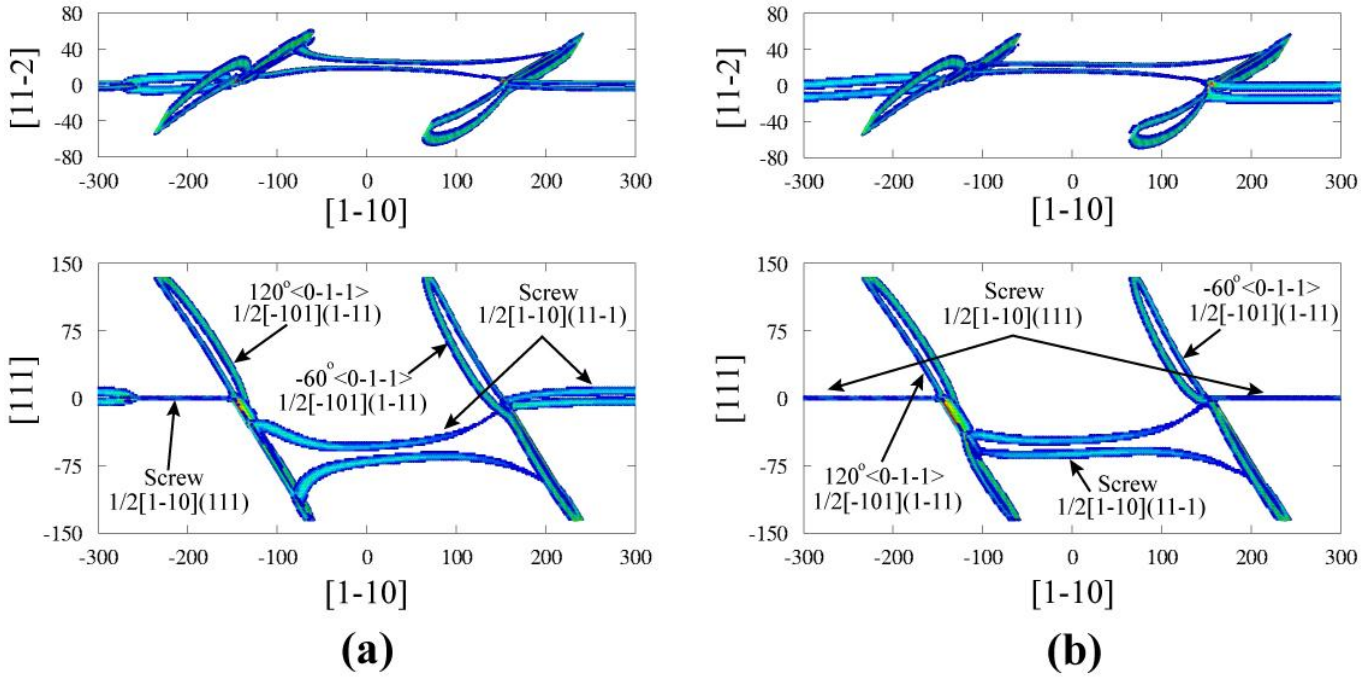
[11-2]
[1-10]
[111]
120°<0-1-1>
1/2[-101](1-11)
-60°<0-1-1>
1/2[-101](1-11)
Screw
1/2[1-10](11-1)
Screw
1/2[1-10](111)
(a)
(b)

Fig. 7:

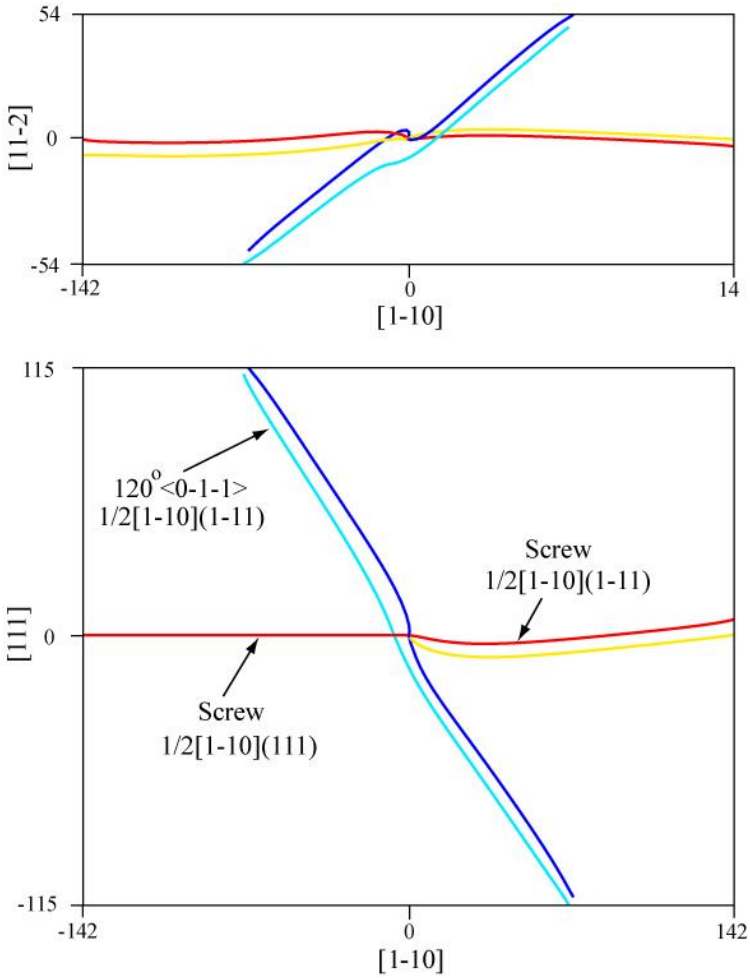
54
0
-54
[11-2]
-142
0
14
[1-10]
115
0
-115
[111]
120°<0-1-1>
1/2[1-10](1-11)
Screw
1/2[1-10](1-11)
Screw
1/2[1-10](111)
-142
0
142
[1-10]

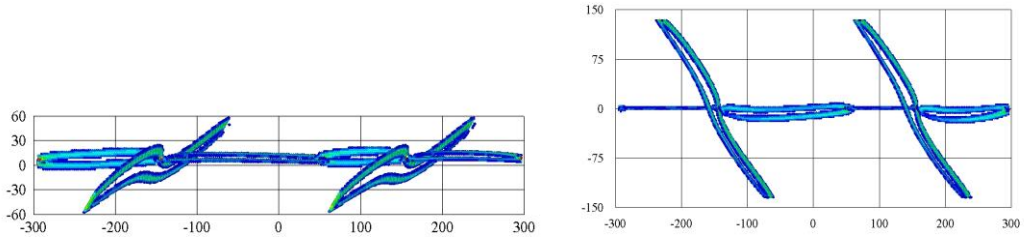
60
30
0
-30
-60
-300
-200
-100
0
100
200
300
150
75
0
-75
-150
-300
-200
-100
0
100
200
300

Fig. 8: